THE 3-D OPTIMIZATION OF AN AXIAL MIXER PROPELLER THROUGH HIGH FIDELITY SIMULATIONS

by

Engin Orcun KOZAKA[a], Pinar DEMIRCIOGLU[b,c*], Ismail BOGREKCI[b], Tarcan ORNEK[a], and Utku KOSE[a,b]

[a] R&D Center of EYS Company, Efeler, Aydin, Turkey
[b] Department of Mechanical Engineering, Faculty of Engineering, Aydin Adnan Menderes University, Aydin, Turkey
[c] Institute of Materials Science, TUM School of Engineering and Design, Technical University of Munich, Garching, Munich, Germany

Original scientific paper
https://doi.org/10.2298/TSCI2304281K

Homogeneous mixing is an important process quality indicator in biogas fermenters for introducing fresh organic feed material to certain bacteria groups such as methanogenic bacteria for anaerobic digestion. Energy consumption for mixing processes is one of the highest operational costs in biogas plants. Thus, it is crucial to carefully consider the energy expenditure per generated thrust (the first performance metric of an axial mixer) for a biogas mixer, since biogas plants are considered as a net carbon zero energy plant. There are several different types of mixers. Axial mixers both high speed and low speed together with paddle mixers are most common among various types of mixers used in fermenter tanks. In this study it is planned to improve conventional axial biogas mixer efficiency using computer aided engineering tools for design and optimization. This goal will be achieved by using a parametric design strategy for blade geometry together with the open source CFD analysis suite OpenFOAM for measuring performance metrics (i.e. power, torque, and thrust). The most efficient design will be chosen from a set of design candidates residing inside a reasonably large parametric state space, via maximizing the thrust to power ratio.

Key words: *submersible mixer, propeller, parametric design, OpenFOAM, manure*

Introduction

In recent years, about 90% of the world's primary energy demand has been met from fossil fuels such as coal, crude oil and natural gas [1, 2]. In the future, the utilization of fossil fuel reserves and their negative effects on the environment require the utilization of RES [2]. In that sense, the rate of technological development and active redesign of renewable energy plants, their sub-components and processes are important. Biogas production and utilization have shown a steady rising trend in recent years. Due to the presence of significant numbers of biogas producers and sellers of plant components in the market, there is a strong demand that is constantly increasing. The so-called anaerobic process of decomposing organic mass by depriving it of oxygen produces a gas mixture called biogas. Biogas can be used directly as a multifunctional energy source such as heating and lighting, as well as converting it into oth-

* Corresponding author, e-mail: pinar.demircioglu@adu.edu.tr

er types of energy such as mechanical and electrical energy. Energy is obtained by burning directly from biogas, which has a high energy value. It can be used as fuel in internal combustion engines and can directly generate mechanical work or electricity.

Expansion of biogas production and utilization has shown a very strong development over the past years. Strong demand, which has been steadily increasing due to the significant number of biogas producers and plant components vendors have established themselves in the market. Biogas is produced during anaerobic degradation of organic matter in different environments such as landfills and biological waste digesters. Methane, used as biofuel for heat and electricity generation, is the main component of biogas and is not only a valuable source of renewable energy, but also a harmful greenhouse gas emitted into the atmosphere [3]. The biogas generation process is a biochemical process. It consists of four stages: hydrolysis, acidification, acetone production, and methane production. In this process, it is obtained efficiently with the harmony of microbial flora and mechanical design.

Mixing of non-Newtonian fluid-flows is used in many applications, especially in the process industry, but also in wastewater treatment or biogas power plants. Wastewater sludge does not behave like a Newtonian fluid, but it behaves such a pseudo plastic fluid [4]. On the other side, Slurries are generally non-Newtonian fluids [5]. Studies on power consumption have shown the importance of the mixers used in increasing process efficiency. In Germany, until the end of the 2012, about 7589 BGP have processed with approximately 3719 MW electrical capacity. The calculations show that 1 billion kWh per year were used for agitation in Germany Biogas Station, if it is considered that the approximately 8% of produced electricity was used for BGP operations and 50% of these energies were spend for agitation [5, 6]. Approximately 200 million € per year was used for agitations at a cost of energy of 0.2 €/kWh. This calculation is clearly demonstrating that the effects of agitations on the profitableness of BGP working [7]. While vertically aligned mixers are preferred in the process industry, wastewater treatment and biogas plants often use mixers with horizontally aligned shafts (*i.e.* axial mixer) [8]. Submersible mixers are vital wastewater treatment machines widely used in urban and rural wastewater treatment farms. Submersible mixers are used in biochemical reactions such as anaerobic digestion, sedimentation, wastewater aeration and more [9]. The main tasks of mixing are to distribute the newly added substrates inside the reactor, release the produced biogas from digestion to the gas tank, smooth out the disruptive temperature and concentration gradients, and in particular prevent both sinking and floating layers [10, 11].

The use of propeller mixers is particularly important for applications with high flow rates [12]. Propeller mixers are usually centrally arranged, but an eccentric location is also possible. They belong to the category of axial fluid machines and are used for turbulent and high viscous fluid-flow. It reaches the typical viscosity value, but propeller agitators also agitate fluids of approximately higher viscosity [12-14]. Agitators with propellers are mostly used in the field of wastewater treatment and biogas power plant technology.

Propeller designs are critical in submersible mixer operation. The power consumption of the mixers used is important for the efficiency of the mixer. However, power consumption is also related to the waste heat generation of the electric motor, and therefore a poorly designed propeller can cause overheating when operating at off design conditions and therefore complete disruption to the mixing process may occur [4].

The submersible pump is a series connection of stages consisting of an impeller and a diffuser [15]. The impellers connected to a single shaft all rotate at the same angular velocity. Although the impellers rotate at a constant angular velocity throughout the pump, the flow structure in each stage differs greatly from the other stages [16]. These differences lead to the

formation of a complex flow structure and thus cause great difficulties in the experimental characterization of the flow field through the pump. Another difficulty in experimental characterization is that the measured values can vary dramatically depending on many parameters such as fluid viscosity-temperature, impeller vane inlet-outlet angle, diffuser vane inlet-outlet angle, vane number, inter-stage distance, surface roughness and so on. The general trend nowadays is to address the aforementioned problems experimentally. Numerical simulations validated with data. This trend has recently in parallel with the development of numerical solution methods in the years, computer capacities is a result of the significant progress achieved.

The study experimentally investigated the effect of intermediate vanes on pump performance in a submersible pump [17]. They conducted their research by considering a total of 12 different configurations of pump impellers with different number of vanes and intermediate vane sizes. As a result of their research, they found that the application of intermediate vanes will provide a limited improvement in pump performance in certain configurations. The study investigated the optimum vane structure for a centrifugal pump using orthogonal experimental and numerical methods [18]. In their research, they designed and modeled 16 different impeller structures using orthogonal table. The study numerically investigated pressure fluctuations as a result of the interaction between the pressure field across the rotating impeller and the pressure field across the fixed diffuser [19]. The simulations were carried out using the 3-DRANS CFD-code (CFX 10). The study aims to develop a methodology for the prediction of hydroacoustic pressure fluctuations caused by rotor-stator interaction in centrifugal pumps. In this study, the optimum design parameters for a diffuser are numerically investigated [20]. In their research, they used the ANSYS-FLUENT package program to solve the Navier Stokes equations in the numerical simulation process. They performed the simulations considering two different diffusers and selected the pressure conversion parameter as the evaluation parameter. In this study, the steady and unsteady radial forces along the pump are investigated experimentally and numerically. The experimental measurements were carried out by means of a pressure scanner and numerical simulations were carried out with the ANSYS-FLUENT package program. The research was carried out within the scope of impellers with two different outlet diameters in the same volume.

Method

Governing equations

The Navier-Stokes equations that governs fluid motions are expressed as the set of the conservation equations of the momentum, the mass and the energy. These sets of equations consist of PDE that show the sum of changes in velocity, pressure, temperature, and density according to time and location in the fluid problem of interest. For modeling the flow around a submersible mixer in a biogas plant, the mass and momentum conservation equations are expressed as:

– Continuity equation:

$$\frac{\partial \rho}{\partial t} + \nabla(\rho V) = 0 \tag{1}$$

– Momentum equation:

$$\rho\left[\frac{\partial V}{\partial t} + V(\nabla V)\right] = -\nabla p + \mu \nabla^2 V + F \tag{2}$$

Because of these equations are non-linear equations which do not have exact solutions, they are solved with using numerical approaches instead of existing a general solution.

The governing equations can be solved by discretizing them using the finite difference, finite element and finite volume methods. With these solutions, maximum efficiency and minimum energy consumption can be provided by optimizing the fluid dynamics parameters of the flow field such as velocity, pressure, turbulent kinetic energy.

Simulation model and boundary conditions

By averaging of a suitable time for the momentum equation, all details that belonging to turbulence in the flow can be ignored. When averaging is applied to both sets of equations which are momentum and continuity equations. The equation sets emerge which known as Reynolds averaged Navier-Stokes equations (RANS). The non-linear terms that created by the turbulence were solved using the *k-Ω* SSt model. In this study, the pimpleFoam and simpleFoam solvers of OpenFOAM are used. Boundary conditions of calculation domain are given in fig. 1.

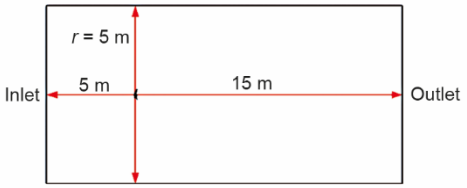

Figure 1. Calculation area and boundary conditions

The Boundary conditions are given as *totalPressure* for pressure at the inlet and *fixedValue* for the outlet. The Boundary conditions for velocity are defined as *pressureInletOutletVelocity* at the inlet, and as *inletOutlet* at the outlet. The Boundary conditions for pressure, velocity, turbulent kinetic energy and *Ω* are given in tab. 1.

Table 1. The boundary conditions for pressure, velocity, turbulent kinetic energy and Ω

Boundaries	*U*	*P*	*k*	*Ω*
Inlet	PressureinletOutletVelocity	TotalPressure	FixedValue	FixedValue
Outlet	InletOutlet	FixedValue	InletOutlet	InletOutlet
FarField	NoSlip	ZeroGradient	KqRWallFunction	OmegaWallFunction
Propeller	NoSlip	ZeroGradient	KqRWallFunction	OmegaWallFunction
AMI rotor/stator	CyclicAMI	CyclicAMI	CyclicAMI	CyclicAMI

Numerical schemes

The numerical discretization schemes which are used to solve the terms in the model of equations in the Open FOAM, are defined in the fvSchemes file. In this file, the numerical schemes that used for solving the terms in the general equations take part according to the OpenFOAM special form. When the gradient terms in the model equation are determined with gradSchemes, the terms that contains divergence and Laplacian are determined with divSchemes and laplacianSchemes respectively. The solution schemes used in the analysis are given in tab. 2.

Since the analysis is a steady-state analysis, the time-derived term is set with ddtSchemes as steady-state. Since there is no problem in terms of the mesh quality, cellLimited Least Square 1 is determined for all gradient terms, in the Gradient Schemes sub-section. The cellLimited Scheme, limits the gradient with extrapolating from the surrounding cells without

falling into the values of other cells. In addition to this, Least Squares is second order, and it calculates the least square distance between all neighbor cells. Also, the value of 1 which has given as a limit, guarantees dependency [21].

Table 2. The Numerical schemes in the fvSchemes

Category	Schemes and values
Time Schemes (ddtSchemes)	steadyState
Gradient schemes (gradSchemes)	cellLimited Least Squares 1
Divergence schemes (divSchemes)	
div(phi,U)	Gauss Upwind
div(phi,k)	Gauss Upwind
div(phi,omega)	Gauss Upwind
div((nuEff*dev2(T(grad(U)))))	Gauss Linear
Laplacian schemes (laplacianSchemes)	Gauss linear corrected
Interpolation schemes(interpolationSchemes)	Linear
Surface normal gradient schemes	Corrected

In the Divergence schemes, the solution schemes of terms containing divergence is determined in the general equation. Gauss Upwind is chosen for the divergence terms U, k, and Ω which in the k-Ω SST turbulence model. Upwind is a recommended schemes under the inaccurate cases that is why it is chosen here. [21]. Stress tensor which is another divergence term is chosen linear as a second order unbounded option.

While the solution scheme of the diffusion term in the momentum equation is chosen as Gauss linear corrected in the LaplacianSchemes, corrected and linear schemes are chosen for Surface Normal gradients interpolation, respectively.

Numerical solution

The settings of equation solver and tolerance are controlled from the fvSolution file in the OpenFOAM [21]. In tab. 3, the selected solver to solve each discretized algebraic equation that exists in the fvSolution file which determined for the analysis, and the smoother settings of this solver are given.

Table 3. The solver and smoother setting in the fvSolution

Variable	Solver	Smoother
Phi	GAMG	GaussSeidel
p	GAMG	DICGaussSeidel
$U\|k$	SmoothSolver	SymGaussSeidel

The Simple algorithm was chosen for pressure-velocity coupling. While the Under-Relaxation Factors values were 0.5 for U, k, and Ω, 0.8 was chosen for the UFinal, the kFinal and the omegaFinal.

Results

Figure 2 shows the field created by a general axial type rotary machine. It is seen that it is directed to the top of the flow by collecting fluid from an area larger than the impeller diameter. This is due to the pressure difference between the suction and pressure side of the propeller. A clearer representation of the pressure difference on the blade is shown in fig. 2(b).

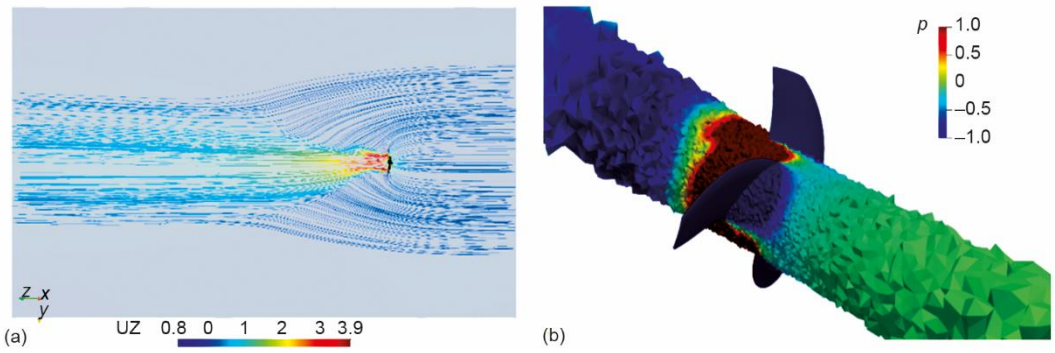

Figure 2. (a) Flow area of axial rotary machine and (b) pressure distribution in cylindrical section

Figure 3 shows the tangentially averaged velocities in the downstream region of the impeller. For tangential, radial and axial velocity, a graph was drawn by taking the velocity at its apse and the value of seven points in the local radii of these cross-sections in its ordinate, separately for all sections at nine different distances from the diameter.

As it can be seen in fig. 3(a), the highest axial velocity was reached at $r/D = 0.25$ at $D/2$ distance. It is seen in fig. 3(b) that this velocity also spreads in the radial direction as it moves in the downstream direction. It can also be seen that the axial velocities in the downstream direction continue at $r/D = 0.75$ up to a distance of 8 D. It can be said that this mixer has not only a directing speed but also an accelerating effect even at 8 D distance. As a matter of fact, it lost its accelerator effect at 10 D and 12 D distances and continued only at a directing speed. Since the axial velocity is the velocity that determines the trust force of the flow, the physical explanation for accelerating the velocities up to 8 D distance in this way is an indication that the flow propelled by the thrust force is accelerated up to that distance.

Another graph to look at to examine propeller performance is the Cp&x/c graph seen in fig. 4. While the abscissa shows the non-dimensionalized distance with the wing axis, the ordinate axis has the Cp value, which shows the pressure difference at that point with respect to the atmospheric pressure. The Cp indicates the suction side on the propeller in negative values and the pressure side in positive values. The slope of the graph shows the pressure change rate and the characteristic of the flow. A straight line indicates that the pressure distribution is smooth and the flow is symmetrical, while an increase in the slope of the curve indicates that there are pressure differences and the flow is asymmetrical. Since the sudden increase of the curve slope indicates a sudden change in the pressure gradient, it should be checked whether there is a flow separation at that point.

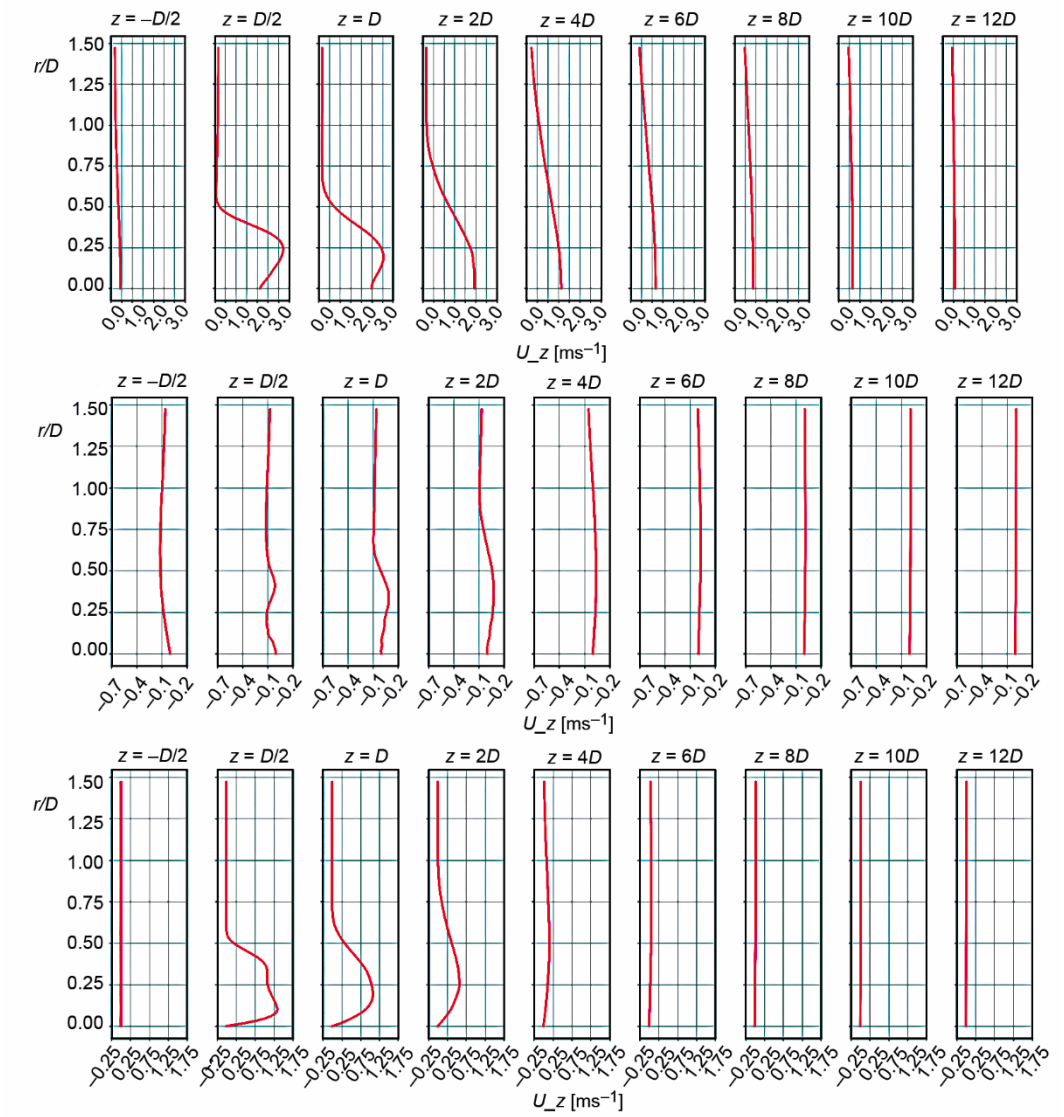

Figure 3. Downstream velocity profiles; (a) axial velocities, (b) radial velocities, and (c) tangential velocities

In fig. 4, four different designs are given: Design0, Design33, Design90, and Design127. These four different designs were selected from the design set as a result of the optimization studies carried out in Caeses, based on thrust, power, torque and thrust produced per power.

In fig. 4, the pressure coefficients of four different designs on the impeller at different *r* sections are given. Pressure coefficient curves of Design0, Design33, Design90, and Design127 are given. As stated before, sudden pressure changes in the *Cp* curve along the chord are undesirable. Another parameter gives the lift coefficient value of the area under the suction side and pressure side curves in the *Cp* graph. The area between the two curves should be

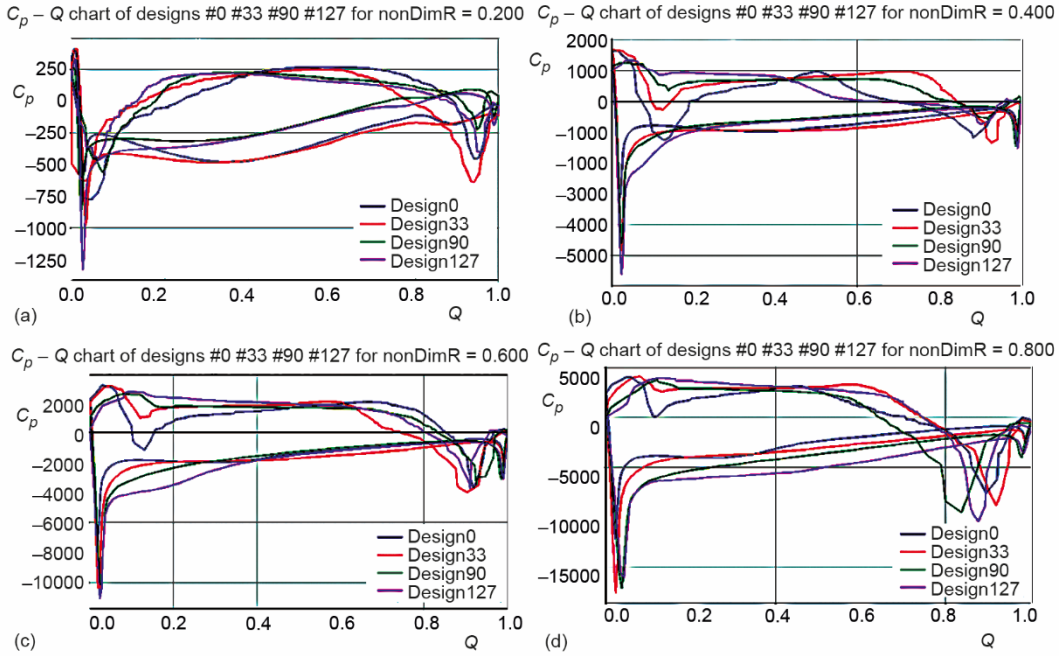

Figure 4. Pressure coefficient distributions in four radial sections of four different designs; (a) *r/R* = 0.2, (b) *r/R* = 0.4, (c) *r/R* = 0.6, and (d) *r/R* = 0.8

maximum, but this means a sudden increase in the pressure gradient, causing flow separations and performance losses. In this case, the most optimum situation for the design should be provided among the options. In fig. 4(a), while the area Design0 is the largest, flow separation may have occurred due to the sudden pressure change close to $\theta = 0.9$. In fig. 4(b), the areas of almost all designs are equal. The design with the largest area in figs. 4(c) and 4(d) is Design127.

References

[1] ***, World Energy Outlook 2019, Available online: https://www.iea.org/reports/world-energy-outlook-2019, (accessed on 15 March 2023)
[2] Ohnmacht, B., *et al.*, Demand-oriented Biogas Production and Biogas Storage in Digestate by Flexibly Feeding a Full-scale Biogas Plant, *Bioresource Technology*, *332* (2021), July, 125077
[3] Rasi, S., *et al.*, Trace Compounds of Biogas from Different Biogas Production Plants, *Energy*, *32* (2021), 8, pp. 1375-1380
[4] Chen, Y. R., *et al.*, Rheological Properties of Sieved Beef-Cattle Manure Slurry: Rheological Model and Effects of Temperature and Solids Concentration, *Agricultural Wastes*, *15* (1986), 1, pp. 17-33
[5] Moeller, G., *et al.*, Rheological Characterisation of Primary and Secondary Sludges Treated by Both Aerobic and Anaerobic Digestion, *Bioresource Technology*, *61* (1997), 3, pp. 207-211
[6] Naegele, H.-J, *et al.*, Electric Energy Consumption of the Full-Scale Research Biogas Plant "Unterer Lindenhof": Results of Longterm and Full Detail Mesaruments, *Energies*, *5* (2012), 12, pp. 5198-5214
[7] Lemmer, A., *et al.*, How Efficient are Agitators in Biogas Digesters? Determination of the Efficiency of Submersible Motor Mixers and Incline Agitators by Measuring Nutrient Distribution in Full-Scale Agricultural Biogas Digesters, *Energies*, *6* (2013), 12, pp. 6255-6273
[8] Reviol, T., *et al.*, Investigation of Propeller Mixer for Agitation of Non-Newtonian Fluid Flow to Predict the Characteristics Within the Design Process, *Chemical Engineering Science*, *191* (2018), Dec., pp. 420-435

[9] Błonski, D., *et al.*, Numerical Simulation and Experimental Investigation of Submersible Sewage Mixer Performance, *Journal of Physics: Conference Series, 1741* (2021), Sept., pp. 1-11
[10] Karim, K., *et al.*, Anaerobic Digestion of Animal Waste: Effect of Mode of Mixing, *Bioresource Technology, 96* (2005), 15, pp. 1607-1612
[11] Kress, P., *et al.*, Effect of Agitation Time on Nutrient Distribution in Full-scale CSTR Biogas Digesters, *Bioresource Technology, 247* (2018), Jan., pp. 1-6
[12] Zlokarnik, M., *Rührtechnik: Theorie und Praxis*, Springer, Berlin, 1999
[13] Kraume, M., *Mischen und Rühren: Grundlagen und moderne Verfahren*, Wiley-VCH, Weinheim, 2003
[14] Reviol, T., *et al.*, A New Design Method for Propeller Mixers Agitating Non-Newtonian Fluid Flow, *Chemical Engineering Science, 190* (2018), Nov., pp. 320-332
[15] Stel, H., *et al.*, Numerical Investigation of the Flow in a Multistage Electric Submersible Pump, *Journal of Petroleum Science and Engineering, 136* (2015), Dec., pp. 41-54
[16] Li, W., *et al.*, Numerical Simulation and Performance Analysis of a Four-stage Centrifugal Pump, *Advances in Mechanical Engineering, 8* (2016), 10, pp. 1-8
[17] Golcu, M., *et al.*, Energy Saving in a Deep Well Pump with Splitter Blade, *Energy Conversion and Management, 47* (2006), 5, pp. 638-651
[18] Zhou, L., *et al.*, Performance Optimization in a Centrifugal Pump Impeller by Orthogonal Experiment and Numerical Simulation, *Advances in Mechanical Engineering, 5* (2013), Jan., pp. 1-7
[19] Berten, S., *et al.*, Rotor-Stator Interaction Induced Pressure Fluctuations: CFD and Hydroacoustic Simulations in the Stationary Components of a Multistage Centrifugal Pump, *Proceedings*, ASME/JSME 2007 5th Joint Fluids Engineering Conference, San Dijego, Cal., USA, 2007, pp. 963-970
[20] Zhou, L., *et al.*, Numerical Investigations and Performance Experiments of a Deep-well Centrifugal Pump with Different Diffusers, *Journal of Fluids Engineering, 134* (2012), 7, pp. 1-8
[21] ***, OpenFOAM Users Guide v10, https://openfoam.org

Paper submitted: January 26, 2023
Paper revised: February 22, 2023
Paper accepted: April 24, 2023